AIAA AVIATION Forum
5-9 June 2017, Denver, Colorado
35th AIAA Applied Aerodynamics Conference

On the Aerodynamic Design of the Hyperloop Concept

Max M. J. Opgenoord* and Philip C. Caplan†
Massachusetts Institute of Technology, Cambridge, MA, 02139

The Hyperloop is a ground-based transportation system concept slated to drastically reduce travel times over medium range distances, for example between San Francisco and Los Angeles. This paper discusses aerodynamic design considerations for the Hyperloop pod. A Hyperloop capsule travels in an unconventional flow regime – very low Reynolds numbers with high Mach numbers – which brings with it unique challenges. This work focuses on the aerodynamic design of the MIT Hyperloop Team. For this design, it is crucial to delay separation over the pod as much as possible by forcing the boundary layer to transition further upstream, resulting in a droplet shape for the aerodynamic shell. We discuss the nominal performance of the aerodynamic design as well as its performance in transonic flow. The overall design of this team's Hyperloop pod won the design competition of the SpaceX Hyperloop Competition in January 2016.

I. Introduction

THE Hyperloop is a concept for high speed ground transportation, consisting of passenger pods traveling at transonic speeds in a partially evacuated tube. The concept was originally proposed in a white paper published by SpaceX in 2013[1] as an alternative to the high-speed rail system currently being developed between Los Angeles and San Francisco, which was deemed too expensive and slow.

The Hyperloop concept could fill a growing need for an alternative transportation mode for short-haul travel. For short routes, such as Los Angeles – San Francisco, or Boston – New York, the time spent traveling at the cruise speed is quite low compared to overall end-to-end travel time due to inescapable inefficencies in air travel (runway taxiing, climb, descent, holding patterns, etc.). The high-frequency throughput of Hyperloop pods could alleviate some of these inefficiencies. Recently, KPMG published a preliminary study commissioned by Hyperloop One – one of the companies commercializing the Hyperloop concept – on the Helsinki–Stockholm corridor where they found that the Hyperloop could cut down end-to-end travel time by 75% to 28 minutes.[2] Furthermore, the market share for high-speed transport is projected to grow rapidly over the next few decades,[3] and the Hyperloop concept could take some pressure off increasingly congested airports and flight routes.

Momentum is growing in the Hyperloop movement, with a number of newly founded companies attempting to commercialize it. In addition, SpaceX is sponsoring a student competition to encourage innovation and to help accelerate the development of a working prototype, starting June 2015[a]. Over 1,000 teams submitted their intent to compete, and over 100 teams made it to Design Weekend in January 2016. The student team from the Massachusetts Institute of Technology – the MIT Hyperloop Team[b] – won first place overall in that design weekend.[4] The aerodynamic design of that team's prototype is the subject of this paper.

Academic research into the Hyperloop concept has focused mostly on system integration. A conceptual sizing tool using the OpenMDAO framework[5] focuses primarily on the aerodynamic and thermodynamic interactions between the pod and tube, with recent work focusing on the energy consumption of the system.[6] The pods for the SpaceX Hyperloop Competition were the first physical prototypes of the Hyperloop concept. Recently, one team reported on their aerodynamic design.[7] For that design, a low-fidelity aerodynamic model

*Graduate student, Department of Aeronautics and Astronautics, Team Lead & Aero/Structures Lead, MIT Hyperloop Team, mopg@mit.edu, Student Member AIAA
†Graduate student, Department of Aeronautics and Astronautics, Aero/Structures Engineer, MIT Hyperloop Team, pcaplan@mit.edu, Student Member AIAA
[a]www.spacex.com/hyperloop
[b]hyperloop.mit.edu

was used to optimize the outer mold line, which was subsequently analyzed using a three-dimensional RANS solution with a turbulence model. This paper describes the approach taken by the MIT Hyperloop Team. For rapid design iterations, we use an axisymmetric viscous/inviscid coupled boundary layer method to accurately predict flow separation and transition. The final design is then analyzed using a three-dimensional CFD solver, which is also used to characterize the aerodynamics at higher velocities to investigate the potential issues related to Hyperloop pods traveling through a partially evacuated tube at transonic speeds.

Section II discusses historic background of the Hyperloop concept, as well as the SpaceX Hyperloop competition. Section III explains the design philosophy chosen by the MIT Hyperloop team, as well as a brief overview of the overall pod design. Section IV then describes the aerodynamic design methodology. Section V focuses on the final aerodynamic design and its performance for different flow conditions. Finally, Section VI concludes the paper.

II. Background

Concepts for high-speed trains in vacuum or evacuated tubes can be traced back as far as 1909, when rocket pioneer Robert H. Goddard proposed high-speed passenger-carrying pods traveling through evacuated tubes.[8] Bachelet introduced the core idea behind magnetically levitating trains as early as 1910.[9] Over the years these ideas have been further refined, for instance by the Rand Corporation in 1972 with their "Very High Speed Transport System".[10]

The Hyperloop Alpha white paper combined several of these historic concepts[1] and spurred a great deal of public interest in the concept, something the earlier ideas were somewhat lacking. This white paper discusses a Hyperloop pod that travels at 1220 km/h in a partially evacuated tube (1/1000th of atmospheric pressure) levitating using air bearings. The use of wheels at these high speeds would be quite problematic because of the massive centripetal forces on them. Air bearings are proposed as a more efficient mechanism, where the pod floats on a thin film of compressed air. In the Hyperloop Alpha concept, this compressed air is supplied by an onboard compressor. Propulsion is provided by a linear induction motor. The benefit of this is that the heavy components are built track-side and the pod only has to carry a rotor which makes the propulsion quite efficient. Furthermore, that same linear induction motor can also be used for braking at the other end of the tube to recover a substantial amount of energy.

The onboard compressor is also used to improve the efficiency of the pod at higher speeds. Once the pod reaches transonic speeds, the flow around the pod will start to choke, i.e. the flow around the pod will become sonic. At this sonic condition – the so-called *Kantrowitz limit*[11] – the mass flow around the pod is at its maximum. Therefore, when the speed is further increased, not all flow can travel around the pod and is therefore collected in front of the pod. The result is a column of air being pushed by the pod throughout its run. That pressure build-up results in significant additional drag. The Hyperloop Alpha concept therefore introduces the on-board compressor to compress the additional flow and suck it through the pod, while at the same time supplying compressed air to the air bearings.

Two years after publishing the Hyperloop Alpha white paper, SpaceX announced the Hyperloop student competition to advance the concepts proposed in that white paper to the next level, while at the same time garnering more interest from students, universities and the general public for the concept. In this competition, students are to design and build Hyperloop pods which are then tested on a 1 mile long, 6 ft diameter tube built by SpaceX. The tube has a flat concrete base on which aluminium (Al 6101) track plates and an aluminium I-beam are installed.

The competition is intentionally kept very open, allowing for a variety of different designs. Taking the levitation concepts as an example, wheels, air bearings, and magnetic levitation are all allowed. The Hyperloop Alpha concept used a linear induction motor to get up to speed. Because such a system requires a great deal of integration between the pod and track, and it is quite hard to handle this integration with a large number of teams, SpaceX provides a pusher vehicle to bring pods up to speed.

The most important scoring criteria for the competition are the overall run time (therefore favoring high cruise speeds and fast braking), and the potential to scale up the technologies used in the competition vehicle to a full-scale Hyperloop vehicle.

III. MIT Hyperloop Design

The competition goal is to advance the Hyperloop concept to the next level by designing technologies that one day could be used in full-scale Hyperloop and by using these technologies in a working Hyperloop prototype. Here we cover the final Top-Level Design of the MIT Hyperloop pod.

The overall goal of the MIT Hyperloop Team within this competition was to design and build a pod that scores well in both aspects of the competition, i.e speed and scalability of systems used. The speed goal favors a lightweight design, while the scalability goal comes back in every aspect of the pod. There are several approaches that could be taken to design for scalability, for instance to design a full Hyperloop pod with a large passenger compartment and scale it down for the competition. The MIT Hyperloop team took the approach of focusing on the most important technologies for the Hyperloop concept, and developing scalable technologies for those. Therefore, a major focus was the scalability of the levitation design, the braking design, and the aerodynamics.

Other major driving requirements for the design were imposed by the team itself. Firstly, the pod had to be built in four months (February 2016 start of manufacturing – May 2016 fully assembled), which meant that simpler/easier-to-manufacture designs were often favored. Secondly, the pod needed to accelerate at $2.4G$ – the maximum proposed acceleration offered by the SpaceX pusher. Finally, the pod had to be robust to changes in performance specifications and track tolerances.

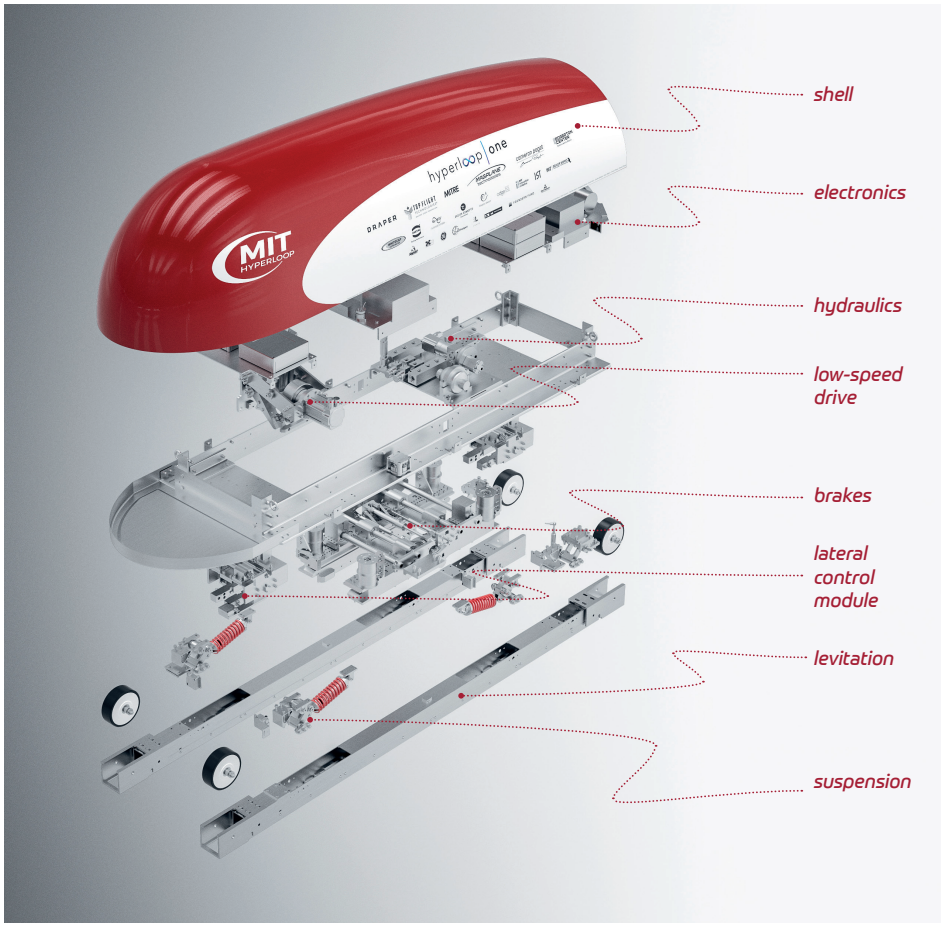

Figure 1. Exploded view of the MIT Hyperloop Design.

An overview of the MIT Hyperloop design is shown in Fig. 1. The prototype is 2.4 m long, weighs 258 kg, and is designed for a top speed of 400 km/h. The pod has no propulsion on board, as we rely on the SpaceX pusher to get up to cruising speed.

Passive magnetic levitation (maglev) is used to levitate above the track, specifically the pod uses an

electrodynamic suspension (EDS) system. Although the original Hyperloop Alpha concept uses air bearings, the track tolerances were poor enough that a large pressure vessel would be required to keep sufficient track clearance ($> 2\ mm$), and it was therefore decided not to use air bearings. EDS works with larger gap heights (on the order of a few milimeters), and additionally becomes more efficient at higher speeds. The levitation system does not require power, therefore it scores well for scalability because of its safety and efficiency at high speeds. Magnetic levitation is notorious for being underdamped, therefore a suspension is added between the magnet arrays and the pod.

The eddy-current braking system uses the same physical principle as the levitation design, only now the design is optimized for drag rather than lift. The design is similar to an eddy-current brake on a rollercoaster. As discussed earlier, linear induction motors will likely be the best technology for propulsion and deceleration. However, track-side infrastructure is required for that. In the case of an anomaly mid-run (e.g. a problem with a pod further down the track, tube de-pressurization/breach, etc.) the pod still has to brake. Therefore, the braking system on the MIT Hyperloop pod is designed as an emergency braking system for a full-scale Hyperloop, decelerating the pod upwards of $2.4G$.

The pod does not have an onboard compressor, both because of the lower speeds in the competition and because the pod does not have air bearings that need to be supplied with air. The Kantrowitz limit will be further discussed in Section V.

IV. Aerodynamic Design Methodology

This section details the design approach used for the aerodynamic shell, and dicusses any analysis tools used in the design.

IV.A. Requirements

The main performance requirement for the aerodynamic shell is to keep the overall $C_D A$ for the pod below 0.5, to adhere to the overall pod run time requirement. Furthermore, the rules require that a dummy is carried in the pod "in a reasonable position" during the test. We chose to use a 3 ft dummy. Other self-imposed requirements are to keep the total weight of any aerodynamic covers below 10 kg, and to be able to access the inside of the pod within 2 minutes.

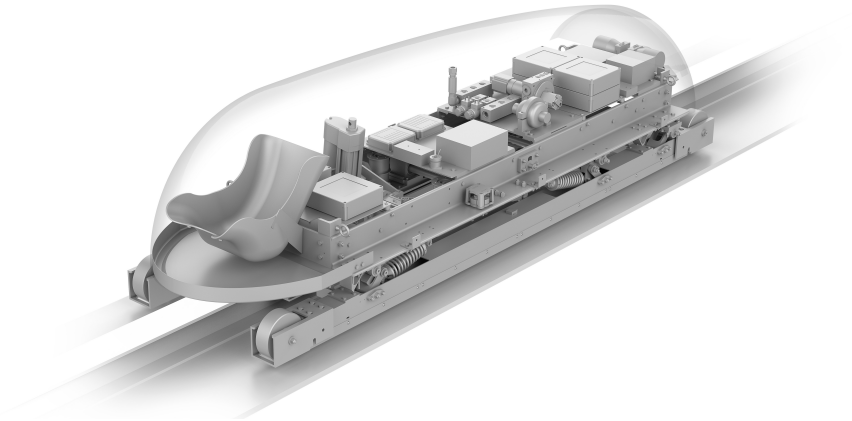

Figure 2. The aerodynamic shell covers the systems inside the pod.

Of course, the aerodynamic shell has to cover the structural frame, while leaving enough room for the dummy, electronics, hydraulics, etc. inside the pod, as shown in Fig. 2. In this case, the other subsystems drive the size of the shell.

IV.B. Flow Regime

The choice of analysis tools for the aerodynamics of this pod depends strongly on the flow regime the pod experiences. Even though the Hyperloop system consists of a large partially evacuated tube, the remaining air in the tube still necessitates a careful aerodynamic design of the outer shape of the pod. Therefore, the

MIT Hyperloop pod has an aerodynamic shell to cover the internals of the pod. To reduce manufacturing risk, the aerodynamic shell is decoupled from the structural frame of the pod, motivated by the aggressive manufacturing timeline in this project.

Because a Hyperloop pod travels at high speed through a partially evacuated tube, it operates in an unconventional flow regime. For the SpaceX Hyperloop competition, the tube pressure is 860 Pa, and the pod will travel at 250 mph. Even though the pressure is quite low, the fluid can still be modeled as a continuum. The Knudsen number Kn is a dimensionless parameter that is typically used to describe the boundary of continuum flow, and is defined as the ratio between the molecular mean free path λ and a characteristic length scale in the flow.[12] For this flow condition, the Knudsen number is $Kn = \mathcal{O}\left(10^{-6}\right)$, which is still far below the continuum limit ($\mathcal{O}\left(10^{-1}\right)$).[13]

The Reynolds number for this flow regime is around 60,000, which means that the flow will transition from laminar to turbulent flow somewhere on the pod. Capturing this transition accurately is crucial and therefore drives the selection of appropriate aerodynamic analysis tools. This Reynolds number is of the same order of magnitude as the full-scale Hyperloop pod in the Hyperloop Alpha paper which travels at a higher speed and is longer, but the pressure in the tube is ten times lower. Finally, the Mach number for the SpaceX Hyperloop competition is around 0.3, requiring compressibility of the fluid to be taken into account. For a full-scale Hyperloop at higher speeds, this Mach number is considerably higher.

As mentioned earlier, the Kantrowitz limit is not significant for this competition due to the lower speeds, and therefore no compressor is included in design analyses.

IV.C. Flow Analysis

During the preliminary design phase, extensive flow analyses are carried out to characterize the design space. Relying on a 3D Navier-Stokes CFD simulation for each design tweak is simply too expensive. Therefore, in the preliminary design phase we relied on an axisymmetric viscous/inviscid analysis code, MTFLOW.[14] Moreover, this viscous/inviscid analysis code allows for capturing transition of the boundary layer from laminar to turbulent accurately, which is critical to the design. MTFLOW is typically used to design axisymmetric bodies and axisymmetric flow passages. This throughflow code uses an integral boundary layer method to solve for the laminar or turbulent boundary layer and a streamline curvature formulation to solve for the inviscid outer flow. The coupling between the inviscid and viscous flow is achieved through the displacement body model. MTFLOW uses the e^n method to capture boundary layer transition.[15,16] We used MTFLOW v2.12, which improves its accuracy of blunt trailing edges.

In order to analyze the final 3D shape of the pod we resorted to a 3D Navier Stokes solver. Unfortunately, these solvers in general are worse at capturing transition than a viscous/inviscid analysis code like MTFLOW.

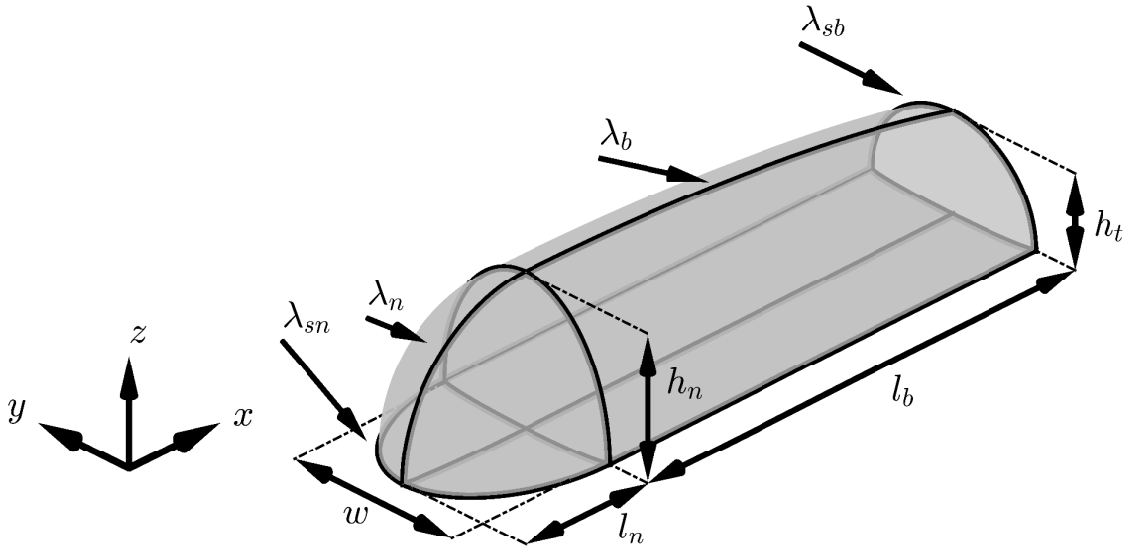

Figure 3. Design parameters for shell geometry.

IV.D. Geometry

To facilitate rapid design iterations, we parametrize the aerodynamic shell in terms of a few geometric parameters, which can be used for trade-off studies. The curvatures in the geometry are generated using Lamé curves. The geometry for the aerodynamic shell as shown in Fig. 3 is parameterized in terms of the overall length of the pod, nose length l_n, width of the pod w, height of the nose h_n, tail height h_t, and the Lamé parameters for the nose λ_n, the side of the nose λ_{sn}, the back λ_b, and the side of the back λ_{sb}.

The geometry shown in Fig. 3 is a three-dimensional geometry, whereas for preliminary design studies we rely on an axisymmetric solver. The conversion from such a three-dimensional geometry to an axisymmetric one is never perfect; for one the pod actually does not travel in the middle of the tube but travels towards the bottom of the tube. The tube is also not perfectly circular because of the concrete base. However, by using a variable axisymmetric tube radius, we can minimize the discrepancies between the axisymmetric and three-dimensional geometries. The variable axisymmetric tube radius is chosen such that the area ratio between the axisymmetric tube and axisymmetric pod is the same as the area ratio between the actual tube and three-dimensional pod. This process is illustrated in Fig. 4. For the axisymmetric shape we revolve the top centerline of the outer mold line on itself.

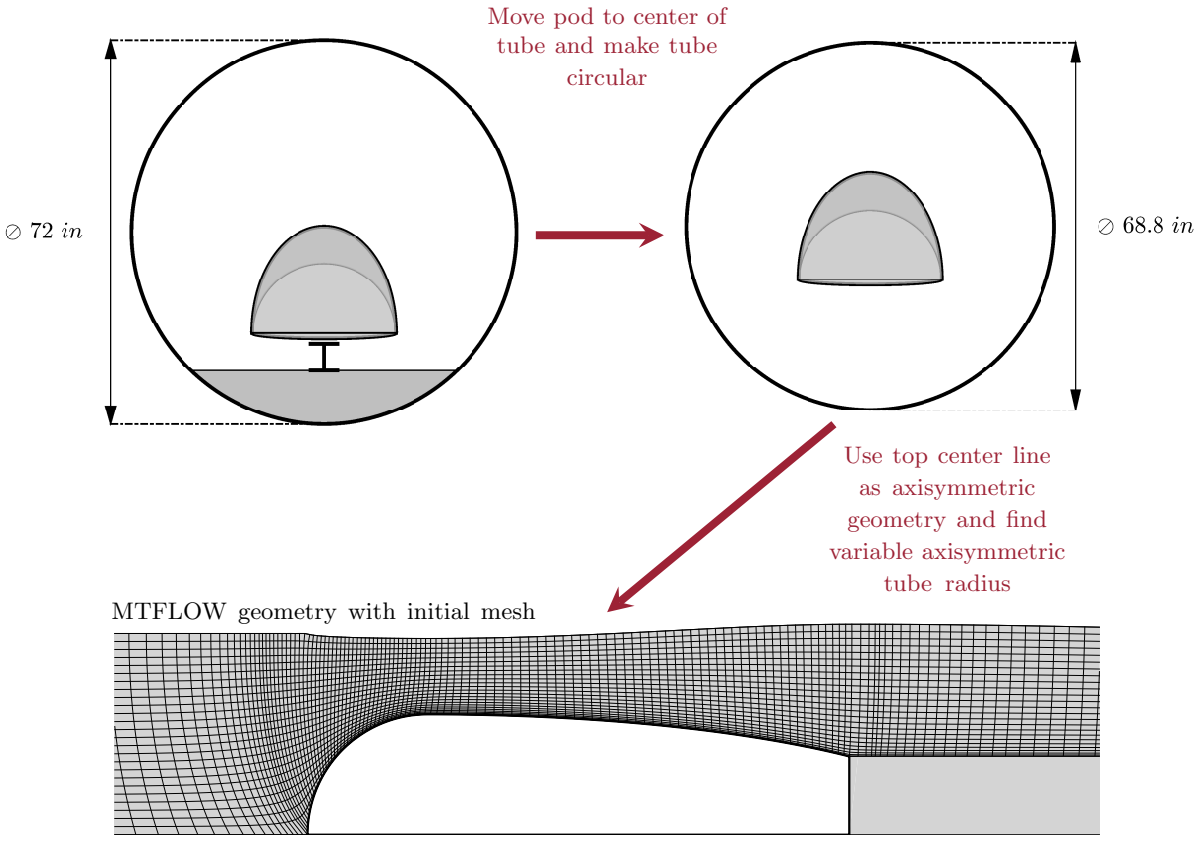

Figure 4. Illustration of recovering the axisymmetric geometry from the full three-dimensional geometry.

V. MIT Hyperloop Aerodynamic Design

The main trade-offs for the aerodynamic design of the MIT Hyperloop pod are discussed in this section. We discuss the final aerodynamic shape, its performance at competition speeds, and characterize its performance at transonic speeds.

V.A. Kantrowitz Limit Considerations

When a pod travels at transonic speeds through a tube, it could choke the flow around the pod. This happens when the Mach number of the flow around the pod is equal to 1. When the pod speeds up further, a large pressure increase in front of the pod results, because the mass flow that can go around the pod is limited. This sonic condition is known as the Kantrowitz limit.[11] There are two main ways to avoid the Kantrowitz limit. The first option is to increase the ratio between tube cross-sectional area and pod cross-sectional area, thereby allowing relatively more air to pass around the pod at a lower velocity. The other option uses a compressor that sucks in air through the front of the pod and feeds the compressed air through a duct in the pod which subsequently exits through a nozzle at the back, which is the approach taken in the Hyperloop Alpha white paper.[1] Neither option is perfect, it either means limiting the cross-sectional area of the pod, hence decreasing payload or increasing tube construction costs, or it means adding an expensive, high-maintenance compressor to each pod. Furthermore, transonic compressors at such low Reynolds numbers would require a large research and development effort, because they are not in use in any aerospace application today.

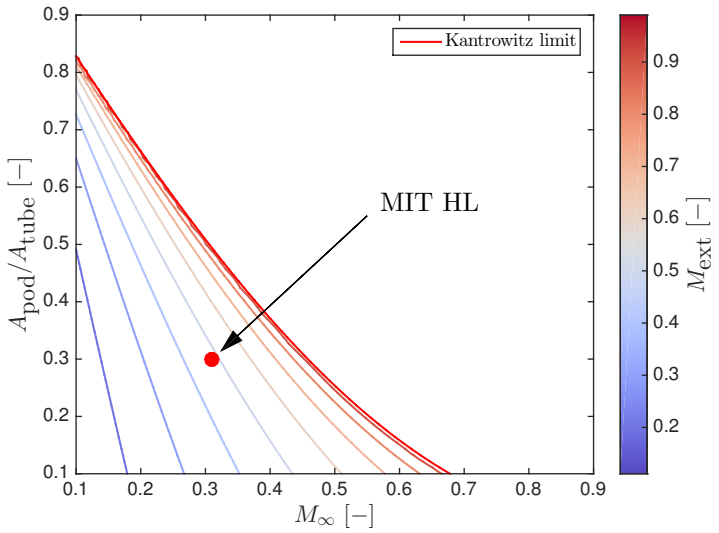

Figure 5. Area ratio (pod-to-tube) versus Mach number. M_{ext} is the maximum Mach number of the flow around the pod – if $M = 1$ the flow is exactly choked. The red line indicates the Kantrowitz limit.

As shown in Fig. 2, the pod does not have a compressor, because it is not worthwhile to use one for the SpaceX Hyperloop competition. Fig. 5 shows the variation of the external Mach number to the pod-to-tube ratio and the freestream Mach number. The external Mach number is the maximum Mach number of the flow around the pod, the flow is choked when that external Mach number equals 1.0. Fig. 5 clearly shows that for a reasonably sized pod without a compressor, the Kantrowitz limits the speed of the pod without an additional drag increase. At an area ratio of 0.3 and a Mach number of 0.3, the flow around the pod is not even close to choking, as seen in Fig. 5. Because compressors also have a large risk associated with them in terms of design, manufacturing, and cost, the MIT Hyperloop team decided not to use a compressor.

V.B. Axisymmetric design

First, an axisymmetric aerodynamic shell was designed using MTFLOW.[14] All of the results in this section are generated using MTFLOW. In the aerodynamic design we relied on sweeps over the design parameters in Fig. 3, rather than going for a purely numerical optimization method. The main reason for this was to gain more physical insight in this design problem with a large unexplored design space, and to use constraints that would be harder to capture in mathematical statements. Additionally, this allowed for a more aggressive design schedule.

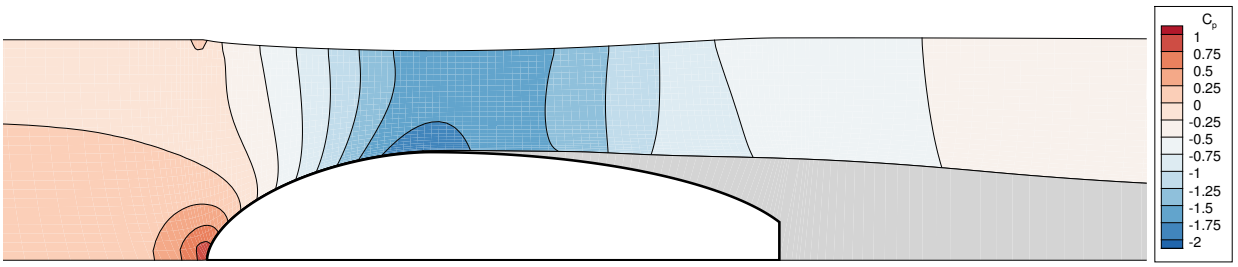

Figure 6. Laminar flow separation on a Hyperloop pod at a Reynolds number $Re = 60,000$ and Mach number $M_\infty = 0.3$. The boundary layer and wake are indicated in gray.

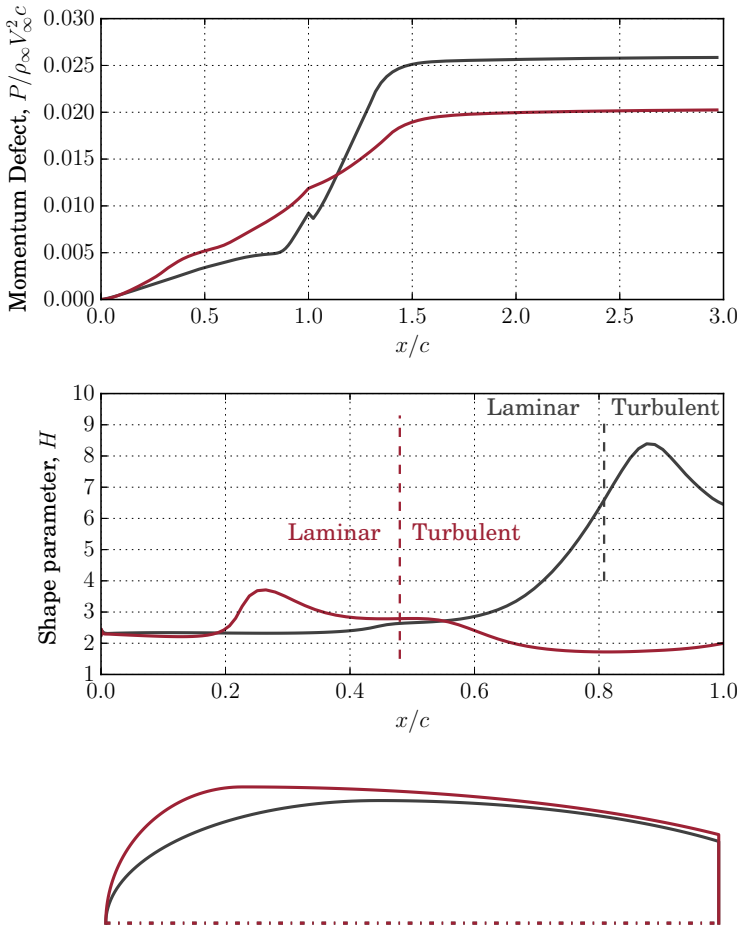

Figure 7. Shape parameter and momentum defect for different dummy positions. The shape in gray positions the dummy in the middle resulting in a flatter shape ($C_D A = 0.0553$), the shape in red positions the dummy in the nose ($C_D A = 0.0431$).

At these low Reynolds numbers ($Re \simeq 60,000$) the boundary layer separates very easily, and proper aerodynamic design is needed to reduce that as much as possible to keep the pressure drag to a minimum. As an example, consider the sleek axisymmetric shape in Fig. 6. The laminar boundary layer separates at a very low adverse pressure gradient – just after the inflection point on the geometry – and therefore this shape results in large amounts of pressure drag. Thus, even though the skin friction drag is low due to laminar flow existing on the surface, the pressure drag is high because of the large wake. This laminar separation has to

be prevented in order to reduce drag. Turbulent boundary layers can handle larger pressure gradients, and a key part to this aerodynamic design is therefore to ensure that the boundary layer transitions to turbulent towards the nose of the pod.

The transition location depends on N_{crit}, which is a measure for the ambient disturbance level as well as some degree of receptivity.[17] Because we expect the environment in the tube to be fairly noisy – e.g. dust in the tube or vibrations due to track disturbances – we use $N_{\text{crit}} = 4$ throughout the design.

The dummy is the largest "component" that has to be fitted inside the shell, and its position is therefore an important consideration in the design of the aerodynamic shell. Here, we show the trade-off between two options. The first option is to put the dummy in the nose of the pod in an upright position, thereby leaving more room for components towards the rear of the pod but resulting in a higher nose. The second option is to lay the dummy more flat over the components inside the pod, thereby reducing the height of the pod and allowing for a more gradual ramp-up to the highest point of the pod.

Fig. 7 shows the results for both of these shapes. For the shape with the dummy in the nose, the boundary layer transitions much closer to the nose, therefore delaying separation and reducing pressure drag. For the shape with the dummy laying flat, the laminar boundary layer separates close to the highest point on the pod, resulting in large pressure drag. Therefore, even though the shape with the dummy in the nose has a larger cross-sectional area, the drag is lower. The reason for this is the blunt nose which is known to promote early transition.[18]

Several different sweeps over design parameters have been performed during the design stage, although only a few of them are discussed here. Fig. 8 shows the influence of the nose Lamé parameter and the tail height on the drag coefficient. When the nose is too shallow (e.g. $\lambda_n = 1.5$) transition will occur later on the pod and more pressure drag results. However, too blunt of a nose increases the curvature on the highest point of the nose, which also induces separation. For the tail height, the higher the tail the higher the pressure drag. However, too low of tail does not add any benefit because the flow separates anyway.

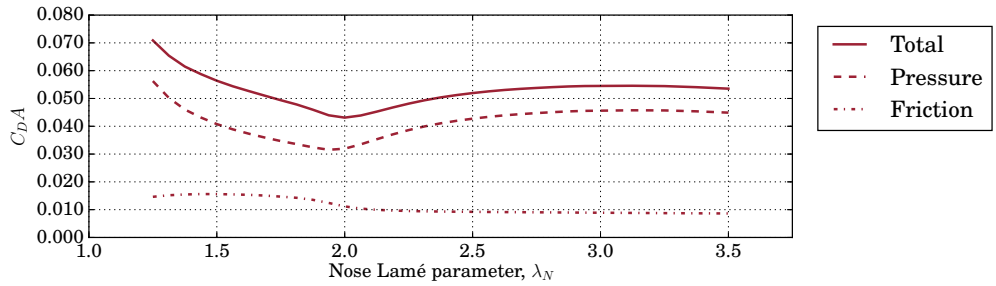

(a) Nose bluntness influence on C_DA for tail height of 12 *in*.

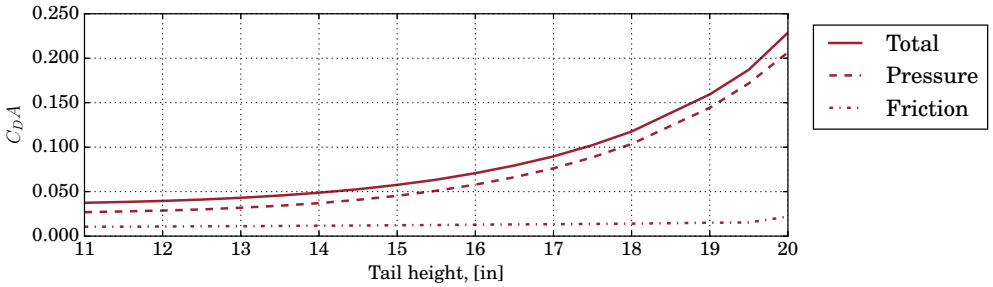

(b) Tail height influence on C_DA for nose Lamé parameter $\lambda_N = 2.0$.

Figure 8. Nose bluntness and tail height influence on drag for axisymmetric pod.

We also investigate the use of an aerodynamic tail section to reduce drag. The idea is to keep a straight section of most of the components on the pod to provide maximum payload capacity, and then add a lightweight aerodynamic tail section to keep drag to a minimum. We compare such a design to our final design in Fig. 9. The concept with an aerodynamic tail has a smaller cross-sectional diameter to keep the

internal volume (excluding tail) similar. The momentum defect on the pod surface is much better for the pod with an aerodynamic tail because there is no adverse pressure gradient on the pod. However, the flow separates as soon as the aerodynamic tail is reached, dramatically increasing the momentum defect. The large increase in pressure drag therefore renders the aerodynamic tail useless.

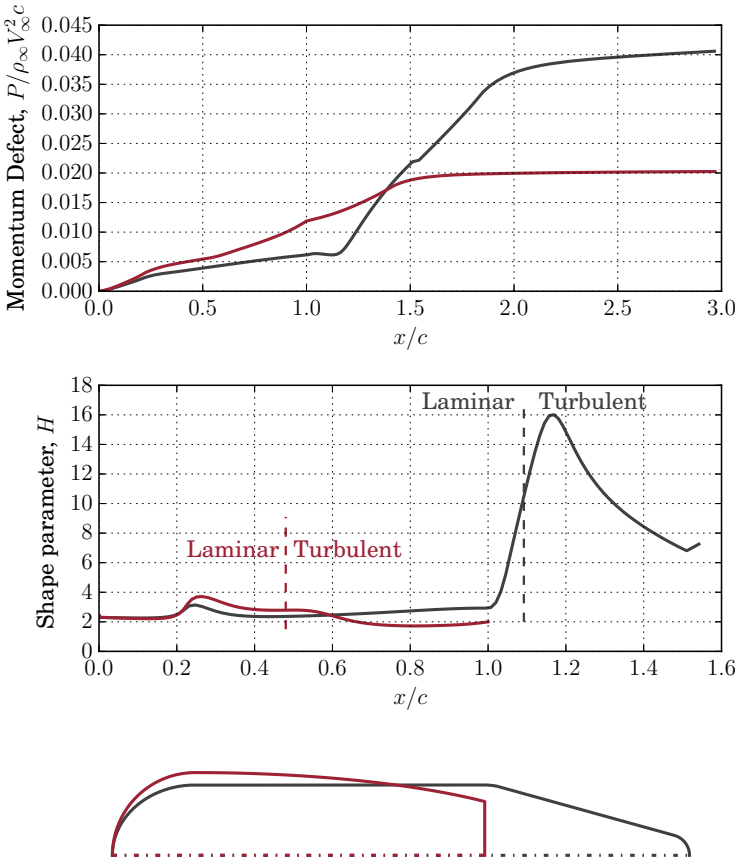

Figure 9. Comparison between designs *with* aerodynamic tail (gray – $C_D A = 0.0950$) and *without* aerodynamic tail (red – $C_D A = 0.0431$).

The flow field around the final geometry is shown in Fig. 10. As mentioned several times, if we can delay separation, we can dramatically reduce the pressure drag, because a turbulent boundary layer can handle adverse pressure gradients much better. Therefore, the final design has a blunt nose section which triggers transition slightly downstream of the tallest point of the pod. This results in no flow separation until the very back of the pod. The back of the pod is not tapered down further, because trying to close it completely (i.e. such that the cross-sectional area of the back is 0) is futile because the flow would separate anyway. Additionally, this shape results in clean separation off the back of the pod, which aids stability, although this is less of a problem here because the ratio of aerodynamic forces to intertial forces on the pod is quite low.

Lastly, we investigate the sensitivity of the performance of the final axisymmetric design to Reynolds number. The variation of drag as a function of Reynolds number is similar to the well-known variation of drag over a cylinder as a function of Reynolds number.[19] The results for low turbulence free stream are computed with $N_{\text{crit}} = 7.0$. We see that the roughness is quite important for the drag of the pod. Trying to trip the boundary layer near the nose could therefore be helpful. This could be achieved by roughening up the nose section. However, Re_θ may not be high enough to effectively use an physical trip on the nose section[c]. In the end, we decided against tripping the boundary layer, because this would require detailed

[c] Re_θ is the Reynolds number based on the momentum thickness of the boundary layer. Transition from laminar to turbulent flow is only possible when locally $Re_\theta \geq 150 \ldots 250$.

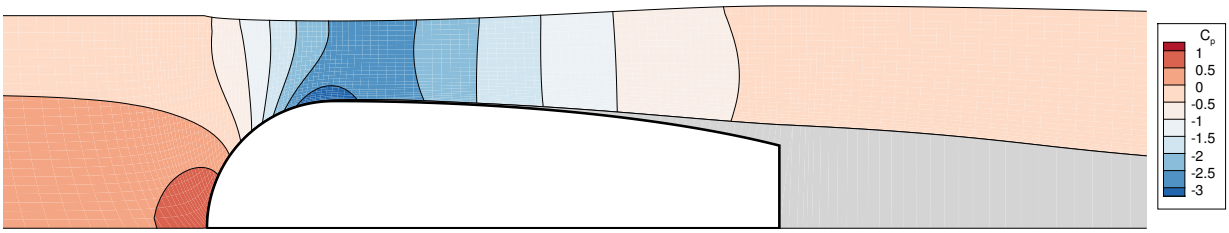

Figure 10. Flow field around the final axisymmetric design at Reynolds number $Re = 60,000$ and Mach number $M_\infty = 0.3$. The boundary layer and wake are indicated in gray.

wind tunnel experiments to get right, and it was decided to spend valuable resources elsewhere instead.

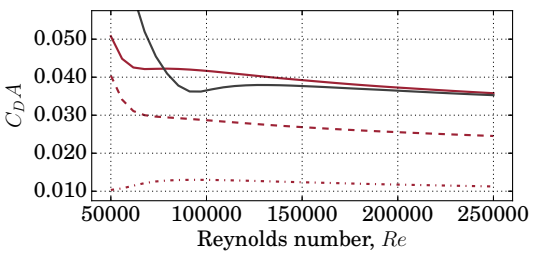

(a) Drag coefficient versus Reynolds number

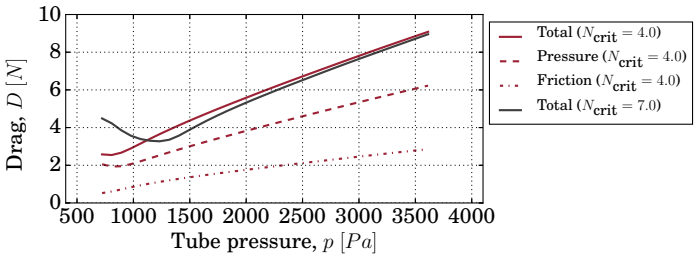

(b) Drag versus tube pressure. Note that the tube pressure is proportional to Reynolds number, because the pod velocity and tube temperature are kept constant here.

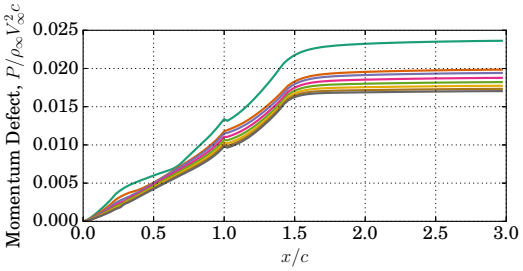

(c) Momentum defect

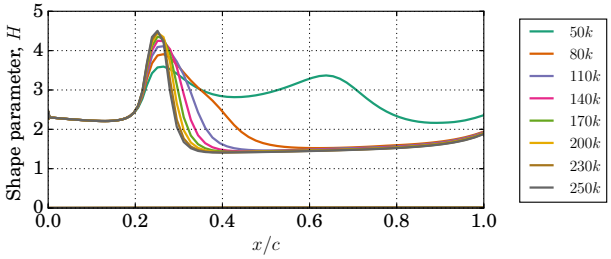

(d) Shape parameter over body

Figure 11. Sensitivity of final axisymmetric shape to Reynolds number.

V.C. Final Three-Dimensional Shape

To generate the three-dimensional shape from the final axisymmetric shape, the axisymmetric shape is used as the centerline for the pod. The other design parameters from Fig. 3 are determined from packaging constraints with the other subsystems (e.g. structural frame, electronics, hydraulics, etc.). We study the performance of this design using STAR-CCM+. For these simulations we solve the laminar Navier-Stokes equations on a very fine grid (2.58 million cells). Adding a turbulence model would overestimate the transition location to be too far upstream and therefore underestimate separation to occur too far downstream. These simulations have to be unsteady because flow separation off the back is an inherently unsteady phenomenon. Total flow conditions (total temperature, total pressure) are set at the inlet to the domain and a pressure outlet is used at the outflow.

The results for the laminar Navier-Stokes simulations over the pod are shown in Fig. 12. We can see a small degree of vortex shedding off the back of the pod, but the overall influence on the drag coefficient is low, as shown in Fig. 12(a). Vortex shedding is to be expected at these low Reynolds numbers.[20] The drag

coefficient is of course quite different from the axisymmetric case due to 3D interference effects. However, the trends that are deduced from the axisymmetric flow results are still valid. We see that the flow over the top of the pod stays attached until the back, agreeing with the axisymmetric results. The drag could be lowered by covering the skis with aerodynamic covers. However, this would reduce accessibility to critical components on the skis, and therefore no aerodynamic covers for the skis are used.

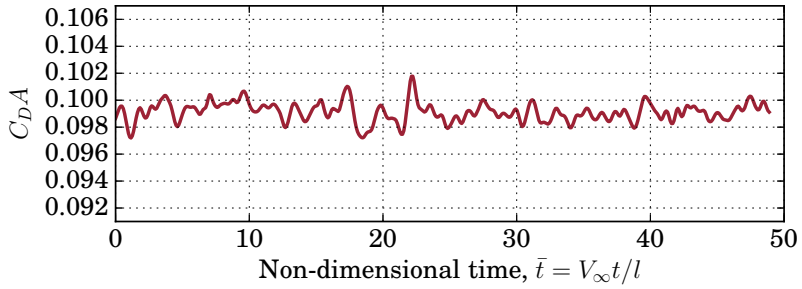

(a) Drag coefficient versus non-dimensional time $\bar{t}$.

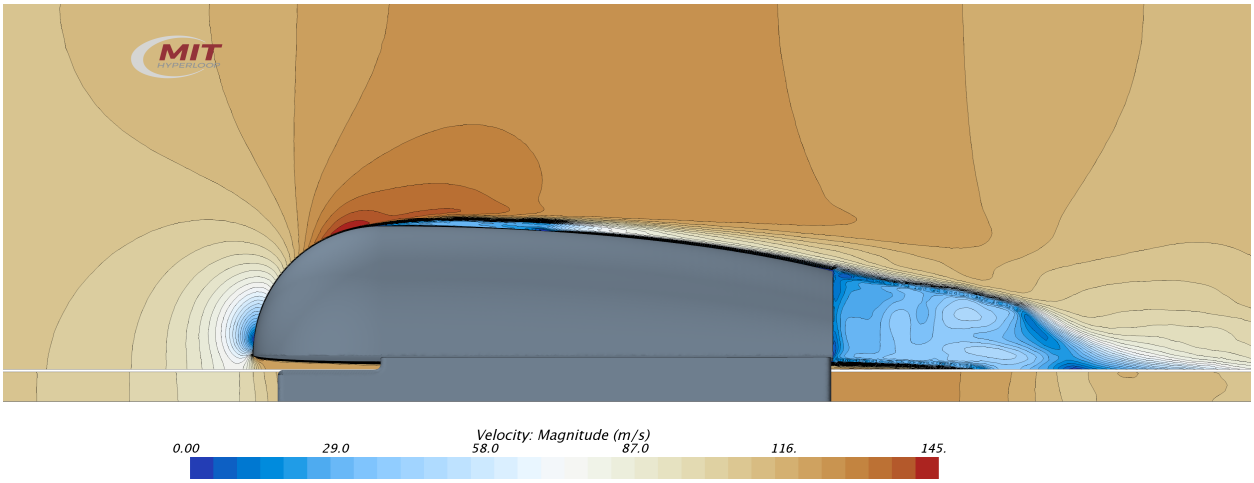

(b) Velocity field contours at $\bar{t} = 48$.

Figure 12. Laminar Navier Stokes solution of the final aerodynamic design 110 m/s ($Re = 60,000$, $M = 0.32$).

V.D. Performance at Transonic Speed

Although the pod will not see any transonic speeds during the competition, we still investigate its performance at higher speeds here because it is such an important part of the Hyperloop concept. In this part of the work, we rely on turbulent 3D Navier-Stokes simulations. At these higher speeds – we increase the pod velocity, thereby increasing both Mach number and Reynolds number – turbulent flow is expected over a larger portion of the pod, and therefore using a turbulence model is more justified. We use the κ-ω SST turbulence model,[21,22] which is known for handling separated flows and adverse pressure gradients well.[23]

Any simulation near and above the Kantrowitz limit has to be unsteady. The choking of the flow around the pod and the subsequent pressure build-up is an inherently unsteady phenomenon, and prevent a steady simulation from converging. This also requires careful set-up of the inlet and outlet boundary conditions, i.e. specifying total pressure and temperature at the inlet, and a pressure outlet at the outflow boundary. Note that the meshes for each run are different to ensure that $y+ \leq 1$ everywhere on the pod boundary.

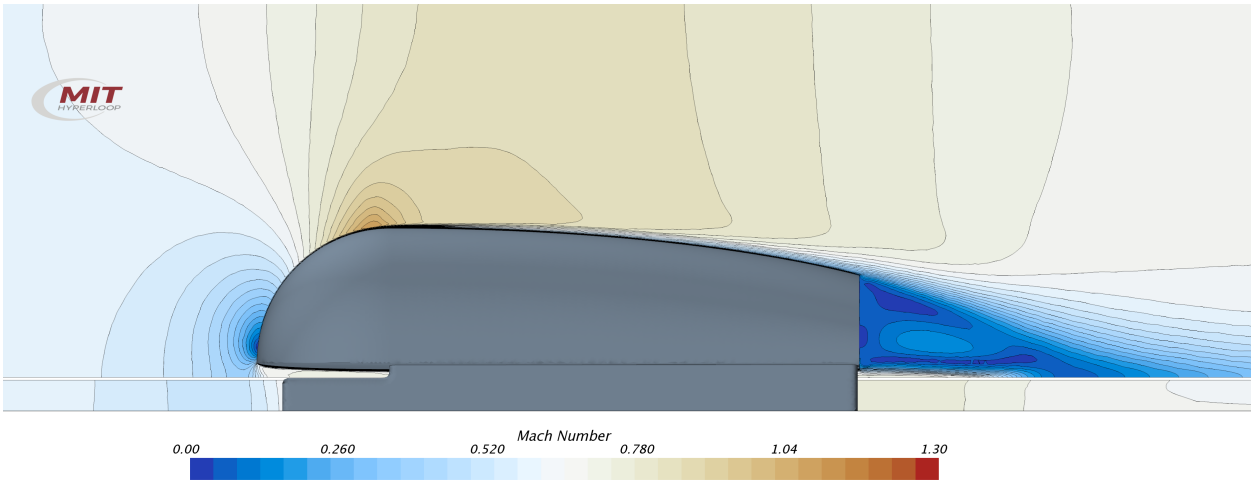

(a) $M_\infty = 0.65$, below Kantrowitz limit.

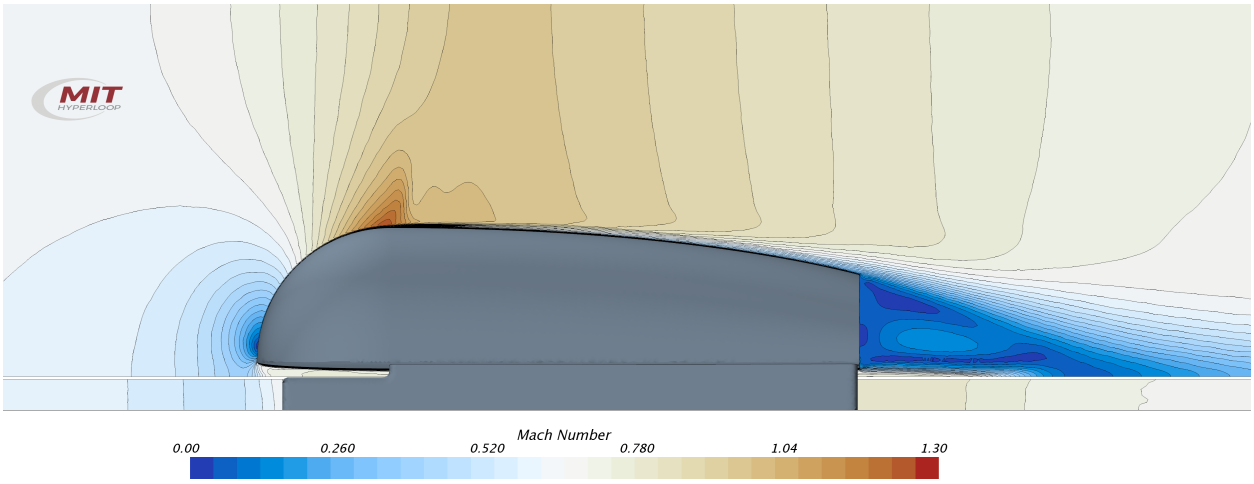

(b) $M_\infty = 0.675$, below Kantrowitz limit, a small shock develops.

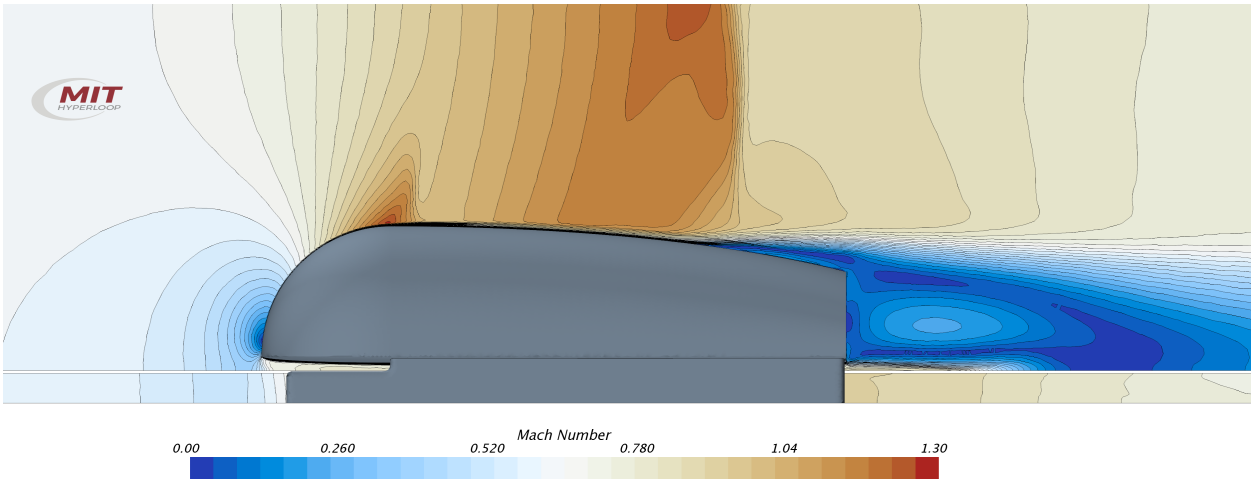

(c) $M_\infty = 0.70$, above Kantrowitz limit.

Figure 13. Contours of local Mach number around the pod for different freestream Mach numbers.

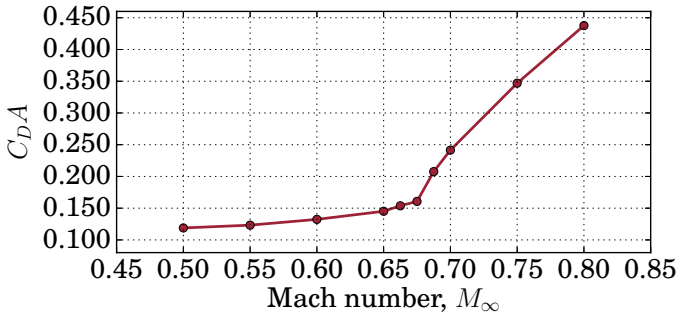

Figure 14. C_DA as a function of Mach number for the final design. The large drag build-up starts around $M_\infty = 0.675$. Note that the freestream density is kept constant, therefore the Reynolds number increases proportionally with Mach number.

The change in C_DA as a function of Mach number is shown in Fig. 14. The small drag increase from $M_\infty = 0.5$ to $M_\infty = 0.65$ can be explained by the flow turning supersonic over the highest point of the pod (as shown in Fig. 13(a)), which results in a small shock with associated wave drag. Although part of the flow over the pod is supersonic at those freestream Mach numbers, the flow has not choked yet, because the supersonic region does not reach all the way to the tube boundaries. The flow around the pod chokes around $M_\infty = 0.675$, resulting in a large drag increase for larger Mach numbers. Due to the fact that not all flow can continue past the pod, a pressure build-up in front of the pod results. Fig. 15 shows the pressure coefficient along the tube, 1 m above the pod, which clearly shows a large pressure increase in front of the pod for freestream Mach numbers higher than 0.675. The drag build-up due to exceeding the Kantrowitz limit is signficant, the drag coefficient is three times as high for $M_\infty = 0.8$ compared to $M_\infty = 0.65$. Note that part of the drag increase is also the result of the wave drag increase due to the associated strong normal shock, as shown in Fig. 13(c). Furthermore, the shock-induced boundary layer separation for $M_\infty > 0.70$ also increases the pressure drag.

The drag increase due to the exceeding the Kantrowitz limit is substantial: a three-fold increase in C_DA between $M_\infty = 0.65$ and $M_\infty = 0.80$. That additional drag increase results in a power loss of 31 kW. However, it is questionable that a compressor used to avoid exceeding the Kantrowitz limit could compress the air to feed it through the pod for less power. For example, the Hyperloop Alpha concept's first stage compressor has a power requirement of 276 kW,[1] and Chin et al. found that for their configuration the compressor power requirement exceeded 300 kW.[5] For our configuration, if we assume an isentropic efficiency for the compressor of 80% and a duct[d] area of 0.05 m^2, the power requirement for the compressor is 204 kW at $M_\infty = 0.80$. Of course, if the power requirement for a compressor to avoid the Kantrowitz limit is higher than the power loss due to the additional drag from exceeding the Kantrowitz limit, adding a compressor would be futile.

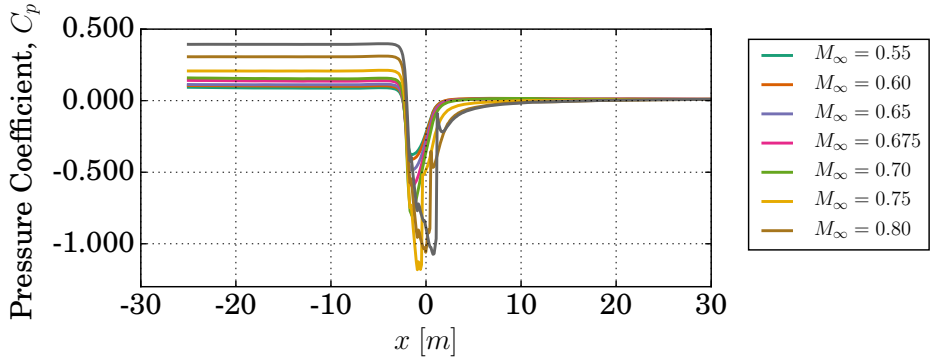

Figure 15. Pressure coefficient at 1 m above the base of the shell along tube for different Mach numbers.

[d]The duct feeds the compressed air from the compressor outlet to the nozzle at the back of the pod.

VI. Conclusion

This paper presented the aerodynamic design of the MIT Hyperloop pod, which participated in the SpaceX Hyperloop Competition from 2015–2017, where it won best overall design at Design Weekend in January 2016. The aerodynamic design strategy was two-fold. First, geometry sweeps were performed using a fast axisymmetric viscous/inviscid analysis tool, while accounting for different flow rates between the axisymmetric and 3D shape. In the aerodynamic design it was crucial to transition the boundary layer to turbulent close to the front of the pod such that higher adverse pressure gradients are tolerated before separation. Such a design strategy increases friction drag but dramatically reduces pressure drag. Once the axisymmetric shape was decided upon, the final three-dimensional geometry was analyzed using a three-dimensional Navier-Stokes solver to characterize its final performance at design speed. Finally, we investigated the performance of the design at transonic speed, where it was found that violating the Kantrowitz limit could lead to three-fold increase in drag coefficient.

Acknowledgements

This engineering project's successful outcome was the result of a massive team effort by the MIT Hyperloop Team, consisting of 35 team members across the Mechanical Engineering, Aeronautical & Astronautical Engineering, and Electrical Engineering & Computer Science departments, as well as the Sloan School of Management. This work could not have been completed without their contribution to the project.

The MIT Hyperloop Team was fortunate to have an array of sponsors, who generously provided advice and funding for this project[e], their support is hereby acknowledged. For this work in particular, Siemens Product Lifecycle Management is thanked for sponsoring the use of STAR-CCM+, as are Main & Partners and Cameron Paget for their help with graphics of the pod. Additionally, we would like to thank SpaceX for organizing and hosting this competition.

Finally, we would like to thank Professor Mark Drela for his initial advice on the aerodynamic design, allowing the use of MTFLOW, and adapting MTFLOW to handle blunt trailing edges better.

References

[1]SpaceX, "Hyperloop Alpha," *SpaceX.(Online Article). http://www.spacex.com/sites/spacex/files/hyperloop_alpha.pdf*, 2013.

[2]KPMG, "Pre-feasibility study Stockhold–Helsinki using Hyperloop One technology – Short summary," `https://home.kpmg.com/content/dam/kpmg/pdf/2016/07/fs-links-pre-feasibility-study-summary.pdf`, July 2016.

[3]Schafer, A. and Victor, D. G., "The future mobility of the world population," *Transportation Research Part A: Policy and Practice*, Vol. 34, No. 3, 2000, pp. 171–205.

[4]Zimmerman, L., "MIT students win first round of SpaceX Hyperloop contest," *MIT News*, February 2016, Accessed 10/23/2016 from `http://news.mit.edu/2016/mit-students-win-first-round-spacex-hyperloop-contest-0201`.

[5]Chin, J. C., Gray, J. S., Jones, S. M., and Berton, J. J., "Open-Source Conceptual Sizing Models for the Hyperloop Passenger Pod," *56th AIAA/ASCE/AHS/ASC Structures, Structural Dynamics and Materials Conference*, Kissimee, Florida, January 5–9 2015.

[6]Decker, K., Chin, J., Peng, A., Summers, C., Nguyen, G., Oberlander, A., Sakib, G., Sharifrazi, N., Heath, C., Gray, J. S., and Falck, R., "Conceptual Sizing and Feasibility Study for a Magnetic Plane Concept," *55th AIAA Aerospace Sciences Meeting*, Grapevine, Texas, January 9–13 2017.

[7]Braun, J., Sousa, J., and Pekardan, C., "Aerodynamic Design and Analysis of the Hyperloop Pod," *52nd AIAA/SAE/ASEE Joint Propulsion Conference*, Salt Lake City, Utah, July 25–27 2016.

[8]Goddard, R. H., "The limit of Rapid Transit," *Scientific American*, Vol. 101, No. 21, 1909, pp. 366.

[9]Bachelet, E., "Levitating transmitting apparatus," March 1912, US Patent 1,020,942. Filed April 2, 1910, *United States of America*.

[10]Salter, R. M., "The very high speed transit system," Tech. Rep. RAND-P-4874, RAND Corporation, Santa Monica, California, 1972.

[11]Kantrowitz, A. and Donaldson, C., "Preliminary investigation of supersonic diffusers," Tech. Rep. Advance Confidential Report L5D20, National Advisory Committee on Aeronautics, Langley Memorial Aeronautical Laboratory, Langley Field, Virginia, 1945.

[12]Knudsen, M., "Die Gesetze der Molekularströmung und der inneren Reibungsströmung der Gase durch Röhren," *Annalen der Physik*, Vol. 333, No. 1, 1909, pp. 75–130.

[13]Chen, G., *Nanoscale energy transport and conversion : a parallel treatment of electrons, molecules, phonons, and photons*, Oxford University Press, New York, 2005.

[e]The full list of sponsors can be found at hyperloop.mit.edu/sponsors.

[14]Drela, M., "A User's Guide to MTFLOW 2.01," Tech. rep., Massachusetts Institute of Technology, Cambridge, MA, 2010.

[15]Van Ingen, J. L., "A suggested semi-empirical method for the calculation of the boundary layer transition region," Tech. Rep. Rapport VTH-74, Technische Hogeschool Delft, Vliegtuigbouwkunde, Delft, The Netherlands, 1956.

[16]Smith, A. M. O. and Gamberoni, N., "Transition, Pressure Gradient, and Stability Theory," Tech. Rep. ES 26388, Douglas Aircraft Co., El Segundo, CA, 1956.

[17]Drela, M., *Flight Vehicle Aerodynamics*, MIT Press, 2014.

[18]Dodbele, S. S., "Effects of forebody geometry on subsonic boundary-layer stability," Tech. Rep. CR NAS1-17919, Vigyan Research Associates, Inc., prepared for the National Aeronautics & Space Administration, Hampton, Virginia, 1990.

[19]Achenbach, E., "Experiments on the flow past spheres at very high Reynolds numbers," *J. Fluid Mech*, Vol. 54, No. 3, 1972, pp. 565–575.

[20]Bearman, P., "On vortex shedding from a circular cylinder in the critical Reynolds number regime," *Journal of Fluid Mechanics*, Vol. 37, No. 03, 1969, pp. 577–585.

[21]Menter, F. R., "Zonal Two Equation $\kappa-\omega$ Turbulence Models for Aerodynamic Flows," *23rd Fluid Dynamics Conference*, July 6–9 1993.

[22]Menter, F. R., "Two-Equation Eddy-Viscosity Turbulence Models for Engineering Applications," *AIAA journal*, Vol. 32, No. 8, 1994, pp. 1598–1605.

[23]Menter, F., Kuntz, M., and Langtry, R., "Ten years of industrial experience with the SST turbulence model," *Proceedings of the Fourth International Symposium on Turbulence, Heat and Mass Transfer*, edited by K. Hanjali, Y. Nagano, and M. J. Tummers, Begell House, 12-17 October 2003.